

Biogenic formation of photoactive arsenic-sulfide nanotubes by *Shewanella* sp. strain HN-41

Ji-Hoon Lee*, Min-Gyu Kim†, Bongyoung Yoo‡, Nosang V. Myung‡, Jongsun Maeng§, Takhee Lee§, Alice C. Dohnalkova¶ James K. Fredrickson¶, Michael J. Sadowsky||, and Hor-Gil Hur*,**

*Department of Environmental Science and Engineering and International Environmental Research Center and †Department of Materials Science and Engineering, Gwangju Institute of Science and Technology, Gwangju 500-712, Republic of Korea; ‡Pohang Accelerator Laboratory, Pohang, Gyeongbuk 790-784, Republic of Korea; ‡Department of Chemical and Environmental Engineering and Center for Nanoscale Science and Engineering, University of California, Riverside, CA 92521; ¶Environmental Molecular Sciences Laboratory and Biological Sciences Division, Pacific Northwest National Laboratory, Richland, WA 99352; and ||Department of Soil, Water, and Climate and BioTechnology Institute, University of Minnesota, St. Paul, MN 55108

Edited by James M. Tiedje, Michigan State University, East Lansing, MI, and approved October 23, 2007 (received for review August 11, 2007)

Microorganisms facilitate the formation of a wide range of minerals that have unique physical and chemical properties as well as morphologies that are not produced by abiotic processes. Here, we report the production of an extensive extracellular network of filamentous, arsenic-sulfide (As-S) nanotubes (20–100 nm in diameter by $\approx 30 \mu\text{m}$ in length) by the dissimilatory metal-reducing bacterium *Shewanella* sp. HN-41. The As-S nanotubes, formed via the reduction of As(V) and $\text{S}_2\text{O}_3^{2-}$, were initially amorphous As_2S_3 but evolved with increasing incubation time toward polycrystalline phases of the chalcogenide minerals realgar (AsS) and duranusite (As_4S). Upon maturation, the As-S nanotubes behaved as metals and semiconductors in terms of their electrical and photoconductive properties, respectively. The As-S nanotubes produced by *Shewanella* may provide useful materials for novel nano- and opto-electronic devices.

Nanotubes are considered critically important building blocks for the production of nanodevices because of their high aspect ratios and unique size-dependent properties (1–3). The former property makes them useful for integration into high-density devices, and the latter, which diverges from the bulk because of quantum confinement effects, helps adjust the electrical and optoelectronic properties by controlling their dimensions for specific applications. Since the first discovery of carbon nanotubes in 1991 (4), there has been growing interest in synthesizing diverse inorganic nanotubes, nanowires, and nanofilms, including metal dichalcogenides, MX_2 ($\text{M} = \text{Mo}, \text{W}, \text{Nb}, \text{Hf}$; $\text{X} = \text{S}, \text{Se}$), which are known to be photoconductive and sensitive to the near-optical-band-gap illumination (5–9). Although chalcogenide As_2S_3 glasses (bandgap = 2.35 eV) are important infrared (IR) transparent materials that have been used in many applications, including waveguides, photonic crystals, sensors, and photolithography (10), there have been no reports of nanotube structures made of arsenic-sulfide that have useful nano- and optoelectronic properties.

Microorganisms play an essential role in the biogeochemical cycling of elements and in the formation of unique minerals (11–14). Biogenic minerals are often formed in the nanometer scale through diverse microbiologically mediated physiological and metabolic activities and by passive surface reactions on cell walls or extracellular structures. They have unique chemical and physical properties (15, 16) as well as diverse morphologies (17, 18) that are not easily duplicated by means of strictly abiotic or synthetic reactions (16). Bacterial dissimilatory metal reduction, for example, can result in the biogenesis of diverse minerals, such as magnetite (Fe_3O_4) (19, 20) and uraninite (UO_2) (21, 22), with unique nanometer-size domains. Because of their small size and large specific surface area, biogenic nanoparticles have found wide use in various medical, biotechnological, chemical, and electronic applications (23).

It was thought that As_2S_3 (orpiment) was formed by abiological processes in nature, chiefly in extreme environments such as in geothermal fluids found in reservoirs and hot springs (24). However, it is now known that the dissimilatory arsenic-respiring

bacterium, *Desulfosporosinus auripigmenti*, formerly *Desulfotomaculum auripigmentum* (25), can precipitate monodisperse, spherical, arsenic trisulfide (As_2S_3) particles, both intra- and extracellularly, under sulfate-reducing conditions (26). Here, we report the microbial production of an extracellular network of filamentous arsenic-sulfide (As-S) nanotubes by *Shewanella* sp. strain HN-41 (27), grown in the presence of As(V) and $\text{S}_2\text{O}_3^{2-}$ under anaerobic conditions.

Results and Discussion

When both As(V) and $\text{S}_2\text{O}_3^{2-}$ were present in the medium, under anaerobic conditions, *Shewanella* strain HN-41 concomitantly reduced As(V) to As(III), and $\text{S}_2\text{O}_3^{2-}$ to S^{2-} (Fig. 1). The concentration of As(III) did not proportionally increase as As(V) was reduced (Fig. 1A), suggesting that As(III) may have been precipitated or became attached to bacterial cells. After inoculation with strain HN-41, the concentration of total sulfide, S^{2-} in the growth medium increased to $279 \mu\text{M}$ by day 2 of incubation, followed by relatively rapid decrease to $29 \mu\text{M}$ by day 7, after which time the concentration S^{2-} remained relatively constant (Fig. 1B). Concomitant with the initial large decrease in the concentration of S^{2-} in the bacterial culture medium was the formation of a yellow-colored precipitate. Preliminary energy dispersive x-ray (EDX) spectral analysis studies indicated that the precipitate consisted of arsenic sulfide (As-S, see below). The As-S precipitates did not redissolve in cultures of strain HN-41, likely because of the relatively low concentration of sulfide. It was shown that a minimum of 1 mM sulfide was required for dissolution of As_2S_3 nanoparticles produced by *D. auripigmenti* (26).

The majority of the aqueous phase S^{2-} was eventually precipitated as arsenic sulfide during the incubation period, as indicated by a trace amount (20–30 μM) of remaining sulfide in the culture media (Fig. 1B). In noninoculated control medium incubated under anaerobic conditions, only a small amount of thiosulfate was reduced to sulfide (Fig. 1B), by an unidentified mechanism, and the aqueous phase sulfide decreased slightly over time because of equilibrium with the head space atmosphere. In contrast to studies showing that relatively acidic conditions lead to the chemical precipitation of As_2S_3 (28), the

Author contributions: J.-H.L., J.K.F., M.J.S., and H.-G.H. designed research; J.-H.L., M.-G.K., B.Y., J.M., A.C.D., and H.-G.H. performed research; A.C.D. and J.K.F. contributed new reagents/analytic tools; J.-H.L., M.-G.K., B.Y., N.V.M., J.M., T.L., A.C.D., J.K.F., M.J.S., and H.-G.H. analyzed data; and J.-H.L., M.-G.K., B.Y., N.V.M., T.L., A.C.D., J.K.F., M.J.S., and H.-G.H. wrote the paper.

The authors declare no conflict of interest.

This article is a PNAS Direct Submission.

Data deposition: The sequence reported in this paper has been deposited in the GenBank database (accession nos. EF580133 and EF580134).

**To whom correspondence should be addressed. E-mail: hghur@gist.ac.kr.

This article contains supporting information online at www.pnas.org/cgi/content/full/0707595104/DC1.

© 2007 by The National Academy of Sciences of the USA

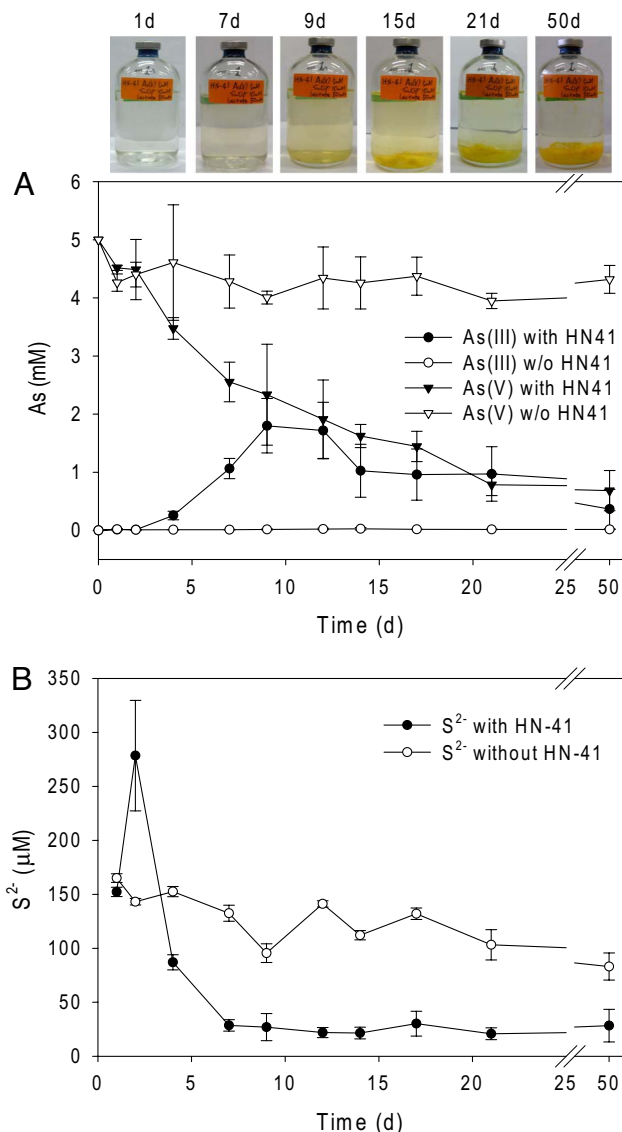


Fig. 1. Concentrations of As (A) and S^{2-} (B) in culture media after incubation with or without *Shewanella* sp. strain HN-41. The incubation bottles at the selected times are shown above A.

culture medium after growth of *Shewanella* strain HN-41 was pH 7.8. Taken together, these results indicate that reduction of As(V) to As(III) and formation of the As-S yellow-colored precipitate was microbiologically mediated by strain HN-41.

Shewanella strain HN-41 did not reduce As(V) when added to the growth medium as the sole electron acceptor [supporting information (SI) Fig. 6A], and only marginal bacterial growth was observed when $S_2O_3^{2-}$ was added to the medium as the sole electron acceptor. Strain HN-41 also grew minimally in the absence of As(V), perhaps because of the toxicity of hydrogen sulfide produced by reduction of thiosulfate. Although there was no detectable S^{2-} in the aqueous phase (SI Fig. 6B), there was an obvious smell of H_2S in the headspace, suggesting that small amounts were generated by reduction of thiosulfate. In the presence of As(V), however, strain HN-41 grew more rapidly, likely because of the removal of H_2S through precipitation as arsenic-sulfide. Thus, under anaerobic conditions, strain HN-41 uses lactate as an electron donor and thiosulfate as the electron acceptor, and the toxic H_2S is likely removed by precipitation as As(III). This was evidenced by the decrease in lactate concen-

tration over time (data not shown), the concomitant production of H_2S from reduction of thiosulfate and production of the As-S yellow-colored precipitate (Fig. 1).

Neither As(III) nor S^{2-} was produced, and there was no reduction of As(V) to As(III), in noninoculated control medium containing As(V) and $S_2O_3^{2-}$ (Fig. 1A and B). Moreover, no yellow-colored precipitate was formed in noninoculated control medium containing either As(V) (5 mM) and S^{2-} (20 mM as $Na_2S \cdot 9H_2O$), or As(III) (5 mM) and S^{2-} (20 mM). Also, no precipitates were formed in kanamycin-treated (50 $\mu g/ml$), uninoculated, supernatant that was collected from the anaerobic incubation of strain HN-41 in LB medium supplemented with either As(V) (5 mM) and S^{2-} (20 mM), or As(III) (5 mM) and S^{2-} (20 mM). Fluorescent staining and confocal laser scanning microscopy indicated that the culture supernatant contained extracellular polymeric substance (EPS) from strain HN-41 (data not shown).

Although bacteria, including *Shewanella*, have been reported to be capable of reducing As(V) by both respiratory and detoxifying reactions (29), the mechanism(s) by which strain HN-41 reduces As(V) is not known. PCR done by using a primer set designed to amplify the internal 242 nt of *arrA*, a well conserved gene that encodes for an enzyme involved in respiratory As(V) reduction, produced only a 206-bp fragment with low sequence similarity (47.1% in 206 of 242 nt) to the *arrA* gene (AY271310) from *Shewanella* sp. strain ANA-3 (30). This suggested that either strain HN-41 has an *arrA* gene that is significantly diverged from the canonical ones found in other bacteria, or it uses a different mechanism for reduction of As(V). Interestingly, however, PCR and subsequent sequence analyses indicated that strain HN-41 contained homologs to *arsB* and *arsC*, an arsenite efflux pump and arsenate reductase, respectively, with deduced protein sequence similarities of 77 and 76.4%, respectively, with the *ArsB* and *ArsC* (AY271310) of *Shewanella* sp. strain ANA-3 (30). Taken together, these results suggest that the growth of strain HN-41 in medium containing both As(V) and $S_2O_3^{2-}$ was likely due to the reduction of $S_2O_3^{2-}$ to S^{2-} , followed by the enzymatic reduction of As(V) to As(III), possibly by the product of the *arsC*. This suggests that strain HN-41 reduces arsenate by means of a detoxification, rather than a respiratory mechanism. The partial sequences of the *Shewanella* sp. HN-41 *arsB* and *arsC* genes have been deposited in GenBank under accession nos. EF580133 and EF580134, respectively.

Electron microscopic analyses of the extracellular, yellow, As-S precipitate formed by strain HN-41 revealed that the material was composed of filamentous structures, with polydisperse diameters ranging from 20 to 100 nm and with lengths up to $\approx 30 \mu m$ (Fig. 2). TEM and EDX image analyses of ≈ 100 cells indicated that no filamentous arsenic-sulfide nanotubes were present intracellularly in *Shewanella* sp. HN-41 (data not shown). Tomographic images taken from a cross-section of the filamentous precipitates exhibited tube-like features in 3D view (Fig. 2C, see also SI Movie 1). TEM of laterally sectioned filamentous precipitates also showed distinct features of nano-scale tubes (Fig. 2B). EDX spectral analysis on a single filamentous nanotube, collected 9 d after inoculation, confirmed the presence of As and S in a ratio of 1:1.5 (SI Fig. 7). This suggested that the filaments were As_2S_3 . The ratio of As/S in samples collected 2–3 wk after inoculation, however, was $1:1.12 \pm 0.05$, which was greater than that of a synthetic arsenic trisulfide standard ($1:1.59 \pm 0.07$) (SI Table 1).

Spatially resolved elemental analyses of cross sections of the As-S nanotubes, done by using scanning-TEM-EDX, revealed that the rim and central regions of the nanotubes had different abundances of As and S (Fig. 2E and F). The concentration of arsenic increased from the central part (point P1) to the rim (point P3), whereas the amount of sulfur decreased from points P1 to P3. Moreover, a greater amount of carbon was detected in the rim, relative to the central region, even after extensive washing with deionized water (SI Fig. 8). Phosphorus, although less abundant, was also distributed

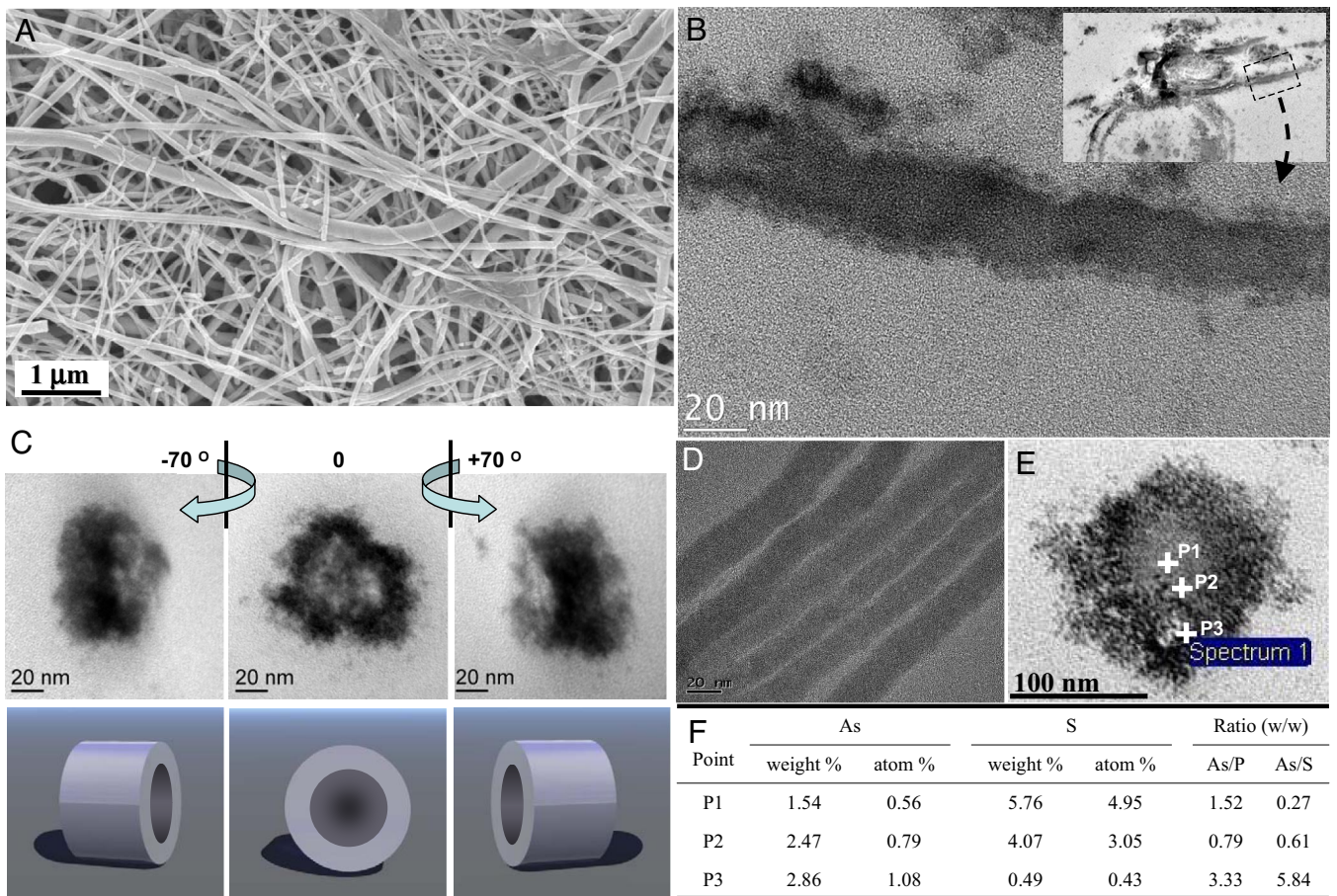


Fig. 2. Electron micrographs of biogenic As-S nanotubes. (A) SEM image. (B) Laterally sectioned TEM images. (Scale bar, 20 nm.) (C) Cross-sectioned TEM tomographs. (D) Whole-mounted TEM image. (E and F) STEM-EDX point spectra from the cross-section of the As-S nanotube.

in a pattern similar to carbon (SI Fig. 8). Although the relative percentages of carbon and phosphorus were higher in the outer parts of the nanotubes than in the inner region (SI Fig. 8), there were not greater absolute amounts of As and S in the inner region. Rather, the relative percentage of As increased toward the rim (Fig. 2F), and similarly, the ratios of arsenic/phosphorus and arsenic/sulfur also increase toward the rim (Fig. 2F). This supports the notion of a tube-like structure with a dense rim region and less-densely structured inner region (Fig. 2 C and E, SI Fig. 8, and SI Movie 1).

Confocal laser scanning microscopic analyses of cell-mineral suspensions stained with fluorescein-labeled PHA-L lectin, SYTO9, or calcofluor provided evidence that the biogenic As-S filamentous nanotubes were intimately associated with an extracellular polymeric substance (EPS). The intense fluorescence staining observed with fluorescently labeled PHA-L (SI Fig. 9A) and bright-field microscopy (SI Fig. 9C) showed that the As-S features, seen as dark spots (SI Fig. 9C), were associated with, or surrounded by, dark gray-colored EPS-containing polysaccharides. In addition, calcofluor staining revealed that EPS was associated with bacterial cells, before the visible precipitation of As-S at day 6 (SI Fig. 10A). Based on these observations, we hypothesize that the EPS formed in the culture medium by strain HN-41 serves as a nucleation core or template for formation of the As-S filamentous nanotubes (SI Tables 2 and 3). This is similar to a previous report suggesting that EPS can act as a template for iron-oxhydroxide filaments (17). There have been several reports that bacterial exopolymers can serve as templates for assembling or precipitating metals as nanoparticulate minerals, including polysaccharides containing iron

oxyhydroxide (β -FeOOH) filaments and filamentous EPS-associated uraninite (UO_2) particles (17, 21, 31). In addition to serving as the template for binding to metals and promoting metal precipitation, it was also suggested that EPS contains *c*-type cytochromes that may serve as the site for the extracellular reduction of U(VI) (21).

The microstructure, crystallinity, and crystal orientation of the As-S filamentous nanotubes were investigated by using x-ray diffraction (XRD) analysis (Fig. 3). The XRD pattern of the nanotubes collected at day 9 showed a broad undefined region, at low angle, with no significant peaks, indicating that the material was amorphous (Fig. 3A). As the incubation time increased, however, several diffraction peaks appeared in the XRD spectra, which were assigned to As_2S_3 (orpiment), and AsS (realgar). The XRD peak intensities also increased with time, indicating that crystallinity of the As-S precipitates improved. In addition, new diffraction peaks at day 50 were also observed that were identified as the arsenic-rich compounds As_4S_3 (dimorphite) and As_4S (duranusite). This result indicates that the ratio of As:S in the precipitates increased with time, resulting in the formation of arsenic-enriched phases. Based on XRD and EDX analyses, the biogenic As-S nanotubes, in association with EPS, are likely undergoing mineralogical alteration from amorphous As_2S_3 to various polycrystalline As-S phases. Considering the standard redox potential of arsenite to elemental arsenic (32) (+0.234 to +0.248 V), the mineralogical changes of the As-S nanotubes are most likely occurring on the surface through abiological processes.

Results in Fig. 4 show the normalized *K*-edge XANES spectra for As and the corresponding Fourier transform (FT) magni-

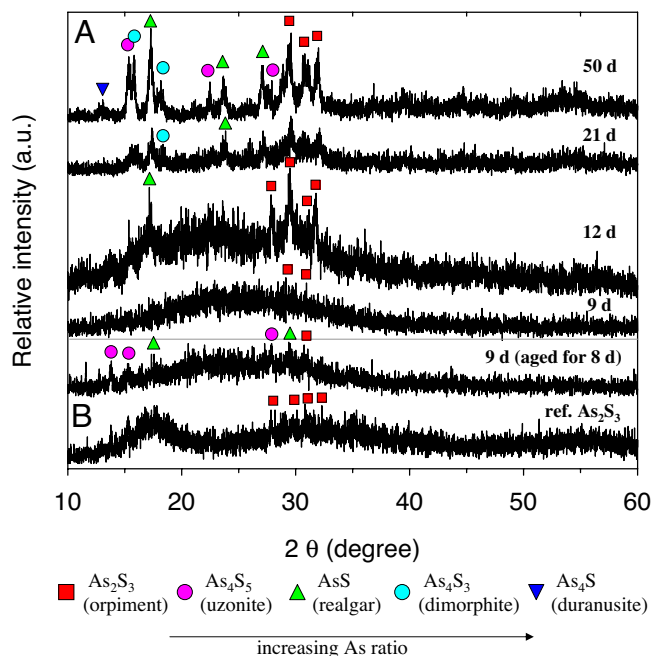


Fig. 3. XRD patterns of the As-S nanotubes. (A) Samples collected at the indicated days. (B) Day 9 samples aged for an additional 8 days under visible light. Commercial reference As_2S_3 is shown below.

tudes of EXAFS spectra for structural evolution of the biogenic As-S nanotubes and those of arsenic reference materials, with respect to incubation time. The XANES spectra (Fig. 4A) revealed that the colloidal As-S complexes contained arsenic predominantly in the +5 oxidation state until day 7, consistent with the relatively smaller amount of aqueous As(III) (Fig. 1A). However, a significant XANES spectral shift for As occurred at day 9, at which time a significant As(III) signal was present in the

precipitates. After 12 days, the As(V) signature abruptly decreased, and the oxidation state of the precipitates was predominantly As(III). The reduction of As(V) to As(III) was complete within 13 days. These spectral results provide key insight into the time-dependent formation of polycrystalline As(III)-S from As(V) and $S_2O_3^{2-}$ that occurs during the microbial reduction process. For the radial structure functions (RSFs) of EXAFS spectra (Fig. 4B), the first FT peak of initial state corresponded to the chemical bonding between As and O. The peak intensity decreased at day 9, and another FT peak appeared at $\approx 1.9 \text{ \AA}$, indicating the occurrence of an As-S chemical interaction (Fig. 4B). The first and second FT peak intensities decreased and increased, respectively, with incubation time. The overall features of the FT peak after day 13 were constant, providing direct evidence for an initial phase change from arsenate to arsenic-sulfide. The evolution of the EXAFS FT peak characteristics, as a function of incubation time, was closely correlated with the shifts observed in the XANES spectra.

The spectral variation seen by using these analyses suggests that the following reactions are involved in the structural evolution of the biogenic As-S nanotubes: the As cluster in the initial culture solution exists mainly as arsenate (AsO_4^{3-}) and is likely “adsorbed” onto HN-41 cells or EPS without a significant change in oxidation state for ≈ 7 days. The electrons produced from the oxidation of lactate by strain HN-41 likely reduce $S_2O_3^{2-}$ to S^{2-} during this period (Fig. 1B), and the detoxification system of strain HN-41 may result in the reduction of adsorbed AsO_4^{3-} to AsO_3^{3-} . After reduction of arsenate is complete, the oxide cluster is replaced by sulfide until day 12, and this is followed by the formation of polycrystalline As-S in association with EPS as a possible template or nucleation site. Although the symmetric single FT peak corresponding to As(III)-S bonding was present in the As_2S_3 standard, all of the biogenic As-S contained another shoulder peak feature at $\approx 2.2 \text{ \AA}$. This is likely because of As-As metallic bonding, as shown in RSF of the reference As metallic powder (Fig. 4B). The EXAFS spectroscopic results support the XRD data (Fig. 3), demonstrating an evolution in mineralogy from amorphous As_2S_3 to a polycrystalline mixture of several As-S phases, resulting in increasing

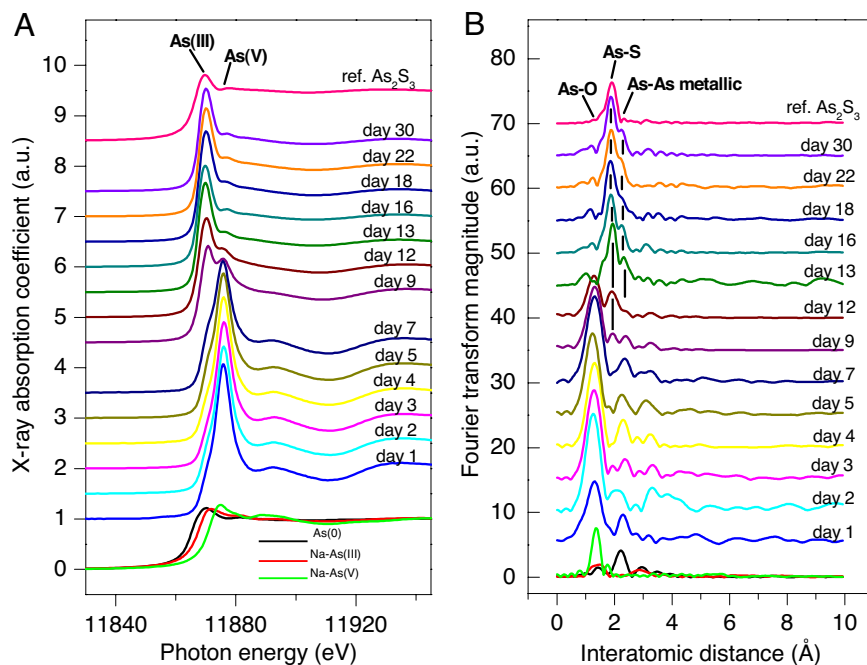


Fig. 4. XANES (A) and Fourier transformed EXAFS (B) As K-edge spectra of reference As-minerals (commercial reference As_2S_3 , elemental As, sodium arsenate, and sodium arsenite) and the biogenic As-S collected at various incubation times.

I-V characteristics

Optoelectronic properties

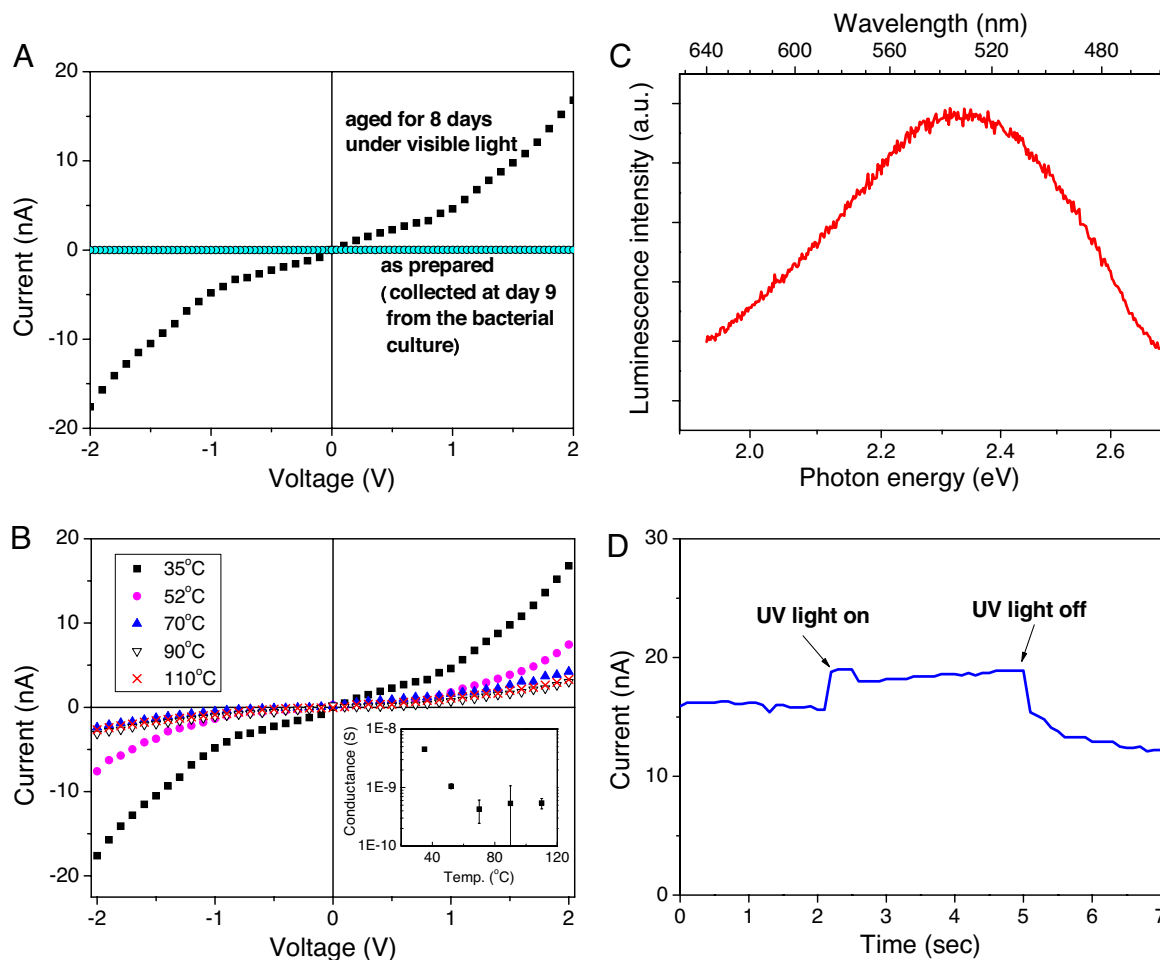


Fig. 5. Electronic and optoelectronic properties of arsenic-sulfide nanotubes produced by *Shewanella* sp. strain HN-41. (A and B) The influence of aging (A) and temperature (B) on I–V characteristics of As–S nanotube networks. (C) Optoelectronic properties of PL spectra (at 25°C). (D) Photocurrent of 9-day-old as prepared As–S nanotubes upon exposure to UV light.

As-rich minerals with incubation time. The EXAFS results are also consistent with EDX and STEM-EDX data, illustrating the heterogeneous distribution of As, a high As density on the rims of the As–S EPS cross-sections (Fig. 2 E and F and SI Fig. 8).

The electrical characteristics of the As–S nanotubes were investigated by measuring the current–voltage (I–V) relationship. As shown in SI Fig. 11, the As–S filamentous nanotubes collected at day 9 showed very low electrical conductance ($< 10^{-12}$ S at 0.5 V bias) (Fig. 5A). However, after aging for an additional 8 d, electrical conductance increased dramatically (Fig. 5A). This suggested that the As–S filamentous nanotubes were functioning as nanowires. Enhanced electrical conductance was attributed to changes in the microstructure and composition of the As–S filamentous nanotubes with aging. As shown in EDX cross-section (Fig. 2 E and F), XRD patterns (Fig. 3), and EXAFS spectra (Fig. 4B), the As-rich phases were observed on the surface of the As–S filamentous nanotubes with increasing incubation time. This strongly implies that the surface of the As–S nanotubes contains highly conductive As–S solid and/or metallic As nanoclusters. The temperature-dependent I–V characteristics of the 8-d-old As–S nanotubes also support this hypothesis. Results in Fig. 5B show that the electrical conductance of the As–S nanotubes decreased with increasing temperature, a characteristic typical of metallic electrical conduction behavior (33). This metal-like behavior may originate from a partial change

of As–S to elemental As on the surface of the nanotubes. Additional changes in electrical conductivity were not observed in samples incubated for longer times (21 or 50 days) (data not shown). The change in conductivity may also have resulted from further mineralogical alteration, such as structural decomposition.

Photoluminescence (PL) spectra were also acquired to gain insight into the optical properties of As–S filamentous nanotubes. Results in Fig. 5C show that 9-day-old As–S nanotubes had a luminescence peak at 2.34 eV (530 nm), consistent with the optical band gap (2.4 eV) reported for standard As_2S_3 bulk materials (34, 35). The photosensitivity of the As–S nanotubes networks was also examined by measuring photocurrent upon exposure to UV light and application of a 1–V bias. The current increased immediately from ≈ 16 to ≈ 18 nA upon exposure to UV light and then decreased to baseline after the UV light was turned off (Fig. 5D). This result showed that the As–S filamentous nanotubes are photoactive.

In summary, the dissimilatory metal-reducing bacterium *Shewanella* sp. strain HN-41 formed long (up to ≈ 30 μm), variable diameter (20–100 nm), extracellular As–S filamentous nanotubes when grown anaerobically in the presence of thiosulfate and arsenate. The As–S nanotubes comprised amorphous As_2S_3 at the early stage of the formation and were subject to mineralogical alterations over time, resulting in the formation of

polycrystalline minerals consisting of different phases of As–S compounds. Moreover, the As–S-filamentous nanotubes behaved as metals and semiconductors in terms of their electrical properties and were photoconductive. We suggest that the biogenic As–S nanotubes may be useful as building blocks for the construction of the next generation of nanoscale optoelectronic materials (36). For this application, however, more detailed physiological and biochemical studies of strain HN-41 are necessary to produce filamentous As–S nanotubes of uniform size and composition.

Materials and Methods

Bacterial Growth Conditions. *Shewanella* sp. strain HN-41 was grown in Hepes-buffered basal medium (27) prepared in an anaerobic condition by boiling and purging with 100% N₂ (37). The medium was adjusted to an initial pH of 7.5 and supplemented with 20 mM lactate (as sodium DL-lactate), 10 mM thiosulfate (Na₂S₂O₃·5H₂O), and 5 mM arsenate (Na₂HAsO₄·7H₂O). Cultures, in sealed serum bottles, were incubated in the dark at 30°C for 3–4 weeks. Methods for analysis of aqueous arsenic and sulfide concentrations, detection of genes involved in As(V) reduction by PCR, confocal laser scanning microscopy (CLSM) with staining techniques, and analyses of extracellular polymeric substances and carbohydrate components are suggested in *SI Materials and Methods*.

Characterization of Materials. TEM tomography was used to determine the spatial features of the ≈80-nm circular projections that were frequently observed in cross-sectioned material. A Tecnai T12 (FEI) transmission electron microscope, equipped with high-tilt stage and automated tomography capability, was used to digitally acquire tilt series from –70° to +70°, at a 1° increment rate. The tilt series were aligned and reconstructed to a 3D volume by using Inspect3D software (FEI). Energy-dispersive x-ray spectroscopy (EDX) analyses were performed at 200 kV with a Hitachi S-4700 FE-SEM and a JEM 2100F HR-TEM for scanning-TEM (STEM). For XAS, arsenic K-edge x-ray absorption spectra were recorded at the BL7C (EC) beamline of a Pohang light source. For samples lacking visible precipitates, possible colloidal As–S com-

plexes were collected by filtering the whole culture medium onto 20-nm-pore-sized filters (Anodisc 47; Whatman). The filters were dried in a glove box and directly used for XAS measurements.

Electrical and Optoelectronic Measurements of the As–S Precipitates. The temperature-dependent electrical conduction properties of the As–S filamentous precipitates, aged for different times, were investigated. To obtain I–V characteristics, a solution containing the As–S filamentous precipitate was dispensed on prefabricated gold electrodes (SI Fig. 11), and the As–S precipitates bridging the electrodes were air-dried. The I–V characteristics were measured by using a semiconductor parameter analyzer (Agilent 4155A; Agilent Technologies), with the range of applied voltage from –2 to +2 V. Measurements were performed in the dark to eliminate interference from photocurrent.

The optical properties of the filamentous As–S nanotubes were investigated by measuring photoluminescence (PL) on silicon substrates. Spectra were acquired at room temperature with the 325-nm line of a focused continuous wave He–Cd laser as an excitation source with a mean 24-mW power. The resulting luminescence spectra were collected from the excited face, dispersed by a double monochromator, and detected by a water-cooled photomultiplier tube, followed by a gated photon counter. The photocurrent of the As–S precipitates was measured by exposing the sample to UV light (360-nm wavelength, 160 W) with a constant bias voltage at 1 V.

ACKNOWLEDGMENTS. We thank Dr. Namjung Jang, Jin-Soo Chang, Dr. Rameshwar Tatavarty, Jinwook Lee, and Soo-Jin Kim for technical assistance and Dr. Robert A. Kanaly and Dr. Yul Roh for helpful advice. A portion of the research described in this article was performed in the Environmental Molecular Sciences Laboratory, a national scientific user facility sponsored by the U.S. Department of Energy's Office of Biological and Environmental Research and located at Pacific Northwest National Laboratory. J.K.F. was supported by the Environmental Remediation Sciences Program, Office of Biological and Environmental Research, U.S. Department of Energy. This study was partially supported by the 21C Frontier Microbial Genomics and Applications Center Program (Ministry of Science and Technology, Republic of Korea) and National Core Research Center Program Grant R15-2003-012-02002-0).

- He H, Tao NJ (2004) in *Encyclopedia of Nanoscience and Nanotechnology*, ed Nalwa HS (American Scientific, Stephenson Ranch, CA), pp 1–18.
- Sapra S, Sarma DD, Sanvito S, Hill NA (2002) *Nano Lett* 2:605–608.
- Duan X, Huang Y, Cui Y, Wang J, Lieber CM (2001) *Nature* 409:66–69.
- Iijima S (1991) *Nature* 354:56–58.
- Kolobov A (2003) *Photo-Induced Metastability in Amorphous Semiconductor* (Wiley-VCH, Berlin).
- Rao CNR, Nath M (2003) *Dalton Trans* 1:1–24.
- Seifert G, Kohler T, Tenne R (2002) *J Phys Chem B* 106:2497–2501.
- Johnson BR, Schweiger MJ, Sundaram SK (2005) *J Non-Cryst Sol* 351:1410–1416.
- Yesugade NS, Lokhande CD, Bhosale CH (1995) *Thin Solid Films* 263:145–149.
- Klocek P (1991) *Handbook of Infrared Optical Materials* (Marcel Dekker, New York).
- Banfield JF, Nealon KH (1997) in *Reviews in Mineralogy*, ed Ribbe PH (The Mineralogical Society of America, Washington, DC), Vol 35, p 448.
- Newman DK (2001) *Science* 292:1312–1313.
- Lowenstam HA (1981) *Science* 211:1126–1131.
- Fortin D (2004) *Science* 303:1618–1619.
- Sweeney RY, Mao C, Gao X, Burt JL, Belcher AM, Georgiou G, Iverson BL (2004) *Chem Biol* 11:1553–1559.
- Oremland RS, Herbel MJ, Blum JS, Langley S, Beveridge TJ, Ajayan PM, Sutto T, Ellis AV, Curran S (2004) *Appl Environ Microbiol* 70:52–60.
- Chan CS, Stasio GD, Welch SA, Girasole M, Frazer BH, Nesterova MV, Fakra S, Banfield JF (2004) *Science* 303:1656–1658.
- Labrenz M, Druschel GK, Thomsen-Ebert T, Gilbert B, Welch SA, Kemner KM, Logan GA, Summons RE, Stasio GD, Bond PL, et al. (2000) *Science* 290:1744–1747.
- Fredrickson JK, Zachara JM, Kennedy DW, Dong H, Onstott TC, Hinman NW, Li S-M (1998) *Geochim Cosmochim Acta* 62:3239–3257.
- Lovley DR, Stolz JF, Nord GL, Phillips EJP (1987) *Nature* 330:252–254.
- Marshall MJ, Beliaev AS, Dohnalkova AC, Kennedy DW, Shi L, Wang Z, Boyanov MI, Lai B, Kemner KM, McLean JS, et al. (2006) *PLoS Biol* 4:1324–1333.
- Suzuki Y, Kelly SD, Kemner KM, Banfield JF (2002) *Nature* 419:134.
- Mandal D, Bolander ME, Mukhopadhyay D, Sarkar G, Mukherjee P (2006) *Appl Microbiol Biotechnol* 69:485–492.
- Eary LE (1992) *Geochim Cosmochim Acta* 56:2267–2280.
- Stackebrandt E, Schumann P, Schuler E, Hippe H (2003) *Int J Syst Evol Microbiol* 53:1439–1443.
- Newman DK, Beveridge TJ, Morel FMM (1997) *Appl Environ Microbiol* 63:2022–2028.
- Lee J-H, Roh Y, Kim K-W, Hur H-G (2007) *Geomicrobiol J* 24:31–41.
- Rochette EA, Bostick BC, Li G, Fendorf S (2000) *Environ Sci Technol* 34:4714–4720.
- Silver S, Phung LT (2005) *Appl Environ Microbiol* 71:599–608.
- Saltikov CW, Cifuentes A, Venkateswaran K, Newman DK (2003) *Appl Environ Microbiol* 69:2800–2809.
- Dohnalkova A, Marshall MJ, Kennedy DW, Gorby YA, Shi L, Beliaev A, Apkarian R, Fredrickson JK (2005) *Microsc Microanal* 11:116–117.
- Stumm W, Morgan JJ (1996) *Aquatic Chemistry* (Wiley-Interscience, New York).
- Dugdale JS (1977) *The Electrical Properties of Metals and Alloys* (Edward Arnold, London).
- Hisakuni H, Tanaka K (1995) *Science* 270:974–975.
- Shah J, Bösch MA (1979) *Phys Rev Lett* 42:1420–1423.
- Mao C, Solis DJ, Reiss BD, Kottmann ST, Sweeney RY, Hayhurst A, Georgiou G, Iverson B, Belcher AM (2004) *Science* 303:213–217.
- Roh Y, Liu SV, Li G, Huang H, Phelps TJ, Zhou J (2002) *Appl Environ Microbiol* 68:6013–6020.